Steeply reflected *ScSH* precursors from the D" region

Martin Schimmel and Hanneke Paulssen

Department of Theoretical Geophysics, Institute of Earth Sciences, Utrecht University, Netherlands

Abstract. We present evidence for precursors to the *ScS* and *sScS* (*SDS* and *sSDS*) phases observed at epicentral distances smaller than 30°. These precursors are intermittently observed in broadband recordings from the six Incorporated Research Institutions for Seismology stations used (western Pacific region and South America). They appear approximately 35–50 s ahead of the *ScS* arrival on the transverse component and are independent of hypocentral depth. The observed precursors are characterized by relatively large amplitudes in the frequency band from 0.05 to 0.2 Hz. A more detailed analysis is restricted to a subsidiary data set from station SNZO (New Zealand). The coherency, frequency dependence, slowness, polarity, and polarization of the precursors are discussed. Many explanations for *SDS* can be rejected, and we conclude that a reflector 180 km above the core-mantle boundary causes these occasionally strong precursors. The large *SDS/ScS* amplitudes at low frequencies require an unrealistically large impedance contrast for a one-dimensional model. We test the possibility of focusing the *SDS* phase by a discontinuity with topography and show that structure with scale lengths of ~19°–25° (1200–1600 km, i.e., larger than the Fresnel zone) can account for large intermittently observed SDS amplitudes with their geometrical reflection points within the same Fresnel zone. This is surprising, since it is often assumed that scale lengths smaller than the Fresnel zone must be responsible for variations within a Fresnel zone. The limited data set permits no conclusions about the global properties of this phase or its implied reflector.

Introduction

The core-mantle boundary (CMB) is the strongest physical and chemical discontinuity inside the Earth: The density and velocity contrasts across this boundary are larger than those at the free surface. With its expected boundary layers (see *Lay* [1989] and *Loper and Lay* [1995] for a review), it plays a major role in the theory of the Earth's dynamics and evolution. The adjacent D" region [*Bullen*, 1950], the lowermost 150-300 km of the mantle, has therefore been of particular interest to geophysicists. Many seismological studies have tried to quantify the properties of D", but the seismic models vary considerably [e.g., *Lay*, 1989]. The velocity gradients above the CMB decrease compared with the overlaying mantle and may even change sign in some regions [*Doornbos and Mondt*, 1979]. A large number of studies using a variety of approaches find evidence for lateral heterogeneities at the D" (see *Young and Lay* [1987] for a review). The observations of reflected *PcP* or *ScSH* precursors at near-grazing incidence are a case in point. (*ScSH* is used to stress that transverse-polarized *ScS* phases are considered.) All studies of *ScSH* precursors are based on near-grazing incidence phases, which are observed at distances ranging from about 70° to 95°. Early evidence of *ScSH* precursors was found by *Mitchell and Helmberger* [1973] and *Lay and Helmberger* [1983]. The latter authors used waveform and travel time information to infer a 2–3% *S*-velocity

discontinuity located about 280 km above the CMB in three different regions. *Young and Lay* [1990], *Weber and Davis* [1990], *Gaherty and Lay* [1992], and *Garnero et al.* [1993], among others, found evidence for similar *S*-velocity discontinuities, while *Cormier* [1985], *Schlittenhardt et al.* [1985], and *Haddon and Buchbinder* [1987] presented alternate explanations for the observed *ScS* precursors. Among the studies that do suggest a discontinuity, the inferred depth varies by as much as 150 km for different regions [*Garnero et. al.* 1993; *Kendall and Shearer*, 1994].

Near-grazing *ScS* precursors from a 2–3% *S*-velocity discontinuity can be detected owing to the critical reflection and constructive interference of reflected and refracted waves. Reflections from such a discontinuity should not be visible on individual seismograms at shorter epicentral distances and, as far as we know, no steep-angle reflected precursors from D" have been reported. In this paper, we present evidence for the existence of such precursors observed at epicentral distances less than 30°. In the following, we will refer to these precursors as *SDS* and *sSDS* phases. We first describe our data and observations and then investigate the effect of reflector topography on the *SDS* phase. It is not our goal to present one (nonunique) model as a final result but to find a mechanism which explains our data as well as related observations from other studies.

Data and Observations

We collected broadband seismograms from six Incorporated Research Institutions for Seismology (IRIS) stations: CTAO (Aus-

tralia), SNZO (New Zealand), MAJO (Japan), CHTO (Thailand), NNA (Peru), and LPAZ (Bolivia) for the years 1991–1994 for events with an epicentral distance $\Delta < 30°$, magnitude $m_b > 5.5$, and depth $h > 120$ km. The source parameters, including location and origin time, were taken from the monthly Preliminary Determination of Epicenters (PDE) bulletins; events with aftershocks or bad quality recordings were discarded. The remaining data were corrected for instrument response and rotated to obtain transverse-displacement seismograms.

On some seismograms, a clear ScSH precursor is observed on the transverse component 35–55 s before the ScS phase. Figure 1 shows four records for different events and stations. The traces have been aligned to the theoretical arrival time of the ScS phase at zero time. In most cases, the precursors on the transverse component are lower in frequency than ScSH and appear to have the opposite polarity of the ScSH phase.

Good quality broadband data for small epicentral distances are sparse, and the number of unambiguous data is further decreased by possible interferences with other phases, such as sS, SS and sSS. We discarded seismograms if these interferences could occur. Also, at distances larger than $28°$, PSS phases are expected on the radial and vertical components which arrive close to SDS. We discarded the data whenever this was the case in order to avoid possibly contaminated transverse components. Our data set is greatly reduced as a result of these constraints.

Although we show here positive observations on single traces, we cannot identify the SDS phase on the largest part of our data owing to a high noise level. Even if subjective, SDS is established at about 1–10% of our recordings. A few ambiguous precursors catch attention since they are coherent with SDS at low frequencies, but they do not show up as a clear phase. Moreover, on some traces with good signal-to-noise ratio, we can hardly identify a precursor. A clear identification of SDS also requires an unambiguous ScSH phase. In some traces, the ScSH phase is quite weak or absent within a certain frequency range. The recording from MAJO (Figure 1a) exemplifies this. Further, the ScSH/ScSV amplitude ratio can be unstable. For instance, it increases from 0.5 at 0.05 Hz to 2 at about 0.5 Hz for the seismogram from LPAZ in Figure 1b. This might be an indicator of source and/or CMB complexity.

Most of the seismograms with a good signal-to-noise ratio and simple ScSH waveform were obtained for station SNZO. Figure 2 shows two more recordings from this station which contain a clear ScSH phase and a low-frequent precursor on the transverse component. Consequently, we confine our detailed analysis to data from SNZO. These comprise 37 events (Table 1) at epicentral distances ranging from $13°–26°$, with hypocentral depths in the range from 120 to 620 km. About 60% of the events have hypocentral depths greater than 400 km. The map depicted in Figure 3 shows the epicentral locations listed in Table 1 and their reflection points at the CMB.

Coherent ScS, sScS, and ScS2 Precursors

Besides precursors to ScS (SDS), precursors to sScS (sSDS) and ScS2 (SDSScS or ScSSDS) are sometimes observed. Figure 4 illustrates two examples with a low-frequent sSDS phase on the transverse components from events 6 and 22. The traces with the sScSH phase (dashed line) have been multiplied by -1 and aligned to zero time with respect to sScS and plotted on top of the corresponding aligned ScS trace (solid line). It can be seen from Figure 4 that the SDS and sSDS phases can be quite coherent at low frequencies. In general, it is difficult to observe sSDS at frequencies larger than 0.1

Hz since the traces become quite noisy, perhaps due to scattering along the three segments of the path through the uppermost mantle and crust. Coherent signal is also visible on the other components, though at different times, and this may be due to near-receiver S-to-P conversions. Here we are interested in the SDS phase only. Figure 5 shows an ScS2 precursor which is quite similar to the SDS phase.

Coherent sSDS and SDS phases are also observed for the stations NNA, MAJO, and LPAZ. Figure 6 demonstrates a good example of coherent ScS, sScS, and ScS2 precursors at low frequencies recorded at station NNA.

Thus we so far can conclude that (1) the existence of the precursor is independent of the take-off angle at the source which excludes near source scattering; (2) SDS and sSDS are related to ScS and sScS, which cancels the misinterpretation of another phase which would either appear before ScS or sScS; and (3) specific near-receiver scattering can likely be excluded by the similarity of the observations from different regions and distances. However, a reflector at about 180 km above the CMB can be invoked to explain the observed precursors.

Stacks and Slowness Determination

A reflector about 180 km above the CMB would cause a normal move-out (NMO) of the differential travel time ($t_{ScS} - t_{SDS}$) of about -6 s at a distance of $24°$ with a differential slowness of about -0.5 s/deg. We checked this result by performing a slant stack of 18 traces with clear and similar ScSH waveforms. The events used for the stack have underlined event numbers in Table 1. We aligned and normalized the ScSH phases and summed the band-passed (0.05-0.2 Hz) seismograms for different differential slownesses. The result is presented as a contour plot in Figure 7. The ScSH phase can easily be identified as the largest minimum at zero slowness and time. The precursor is clearly visible at about -43 s for a differential slowness between 0.3 and -0.7 s/deg. Its maximum in amplitude is at about -0.5 s/deg. The timing is correct for a discontinuity at about 180 km above the CMB, and although the differential slowness is much less well resolved, the theoretical value of -0.5 s/deg is within the slowness range given by the data.

The epicentral distances of the 18 events used range from $15.3°$ to $25.6°$ but cluster around $22°$. Figure 8 shows stacks for each component at a slowness of -0.5 s/deg and the stacked ScSH waveforms at zero slowness. The line thickness represents the standard deviation of the stack, i.e., the 66% confidence limits, thus a thinner line indicates better-constrained amplitudes. The ScSH phase at zero slowness is a case in point; the thin lines indicate the high similarity of the ScSH signals used. The precursor is strongest on the transverse component, and the radial and vertical components show little and no visible energy, respectively.

A ScS precursor generated close to the receiver must arrive as a P wave in order to shorten the ScS travel time; these are ScSdP or ScSdp-type phases where "d" represents the conversion depth. Such phases lead to onsets which are expected to be strongest or at least present on the vertical component. However, both slant stacks and single traces clearly show the strongest energy on the transverse component. For similar reasons, i.e., absence of clear signals on the radial components, $Sp_{diff}S$ type phases can be excluded as explanations for the precursors.

SDS/ScSH Amplitude Ratio

The theoretical SH reflection coefficient of the CMB without topography equals 1 and is independent of frequency and incidence angle, while for a realistic value of a plane discontinuity within D"
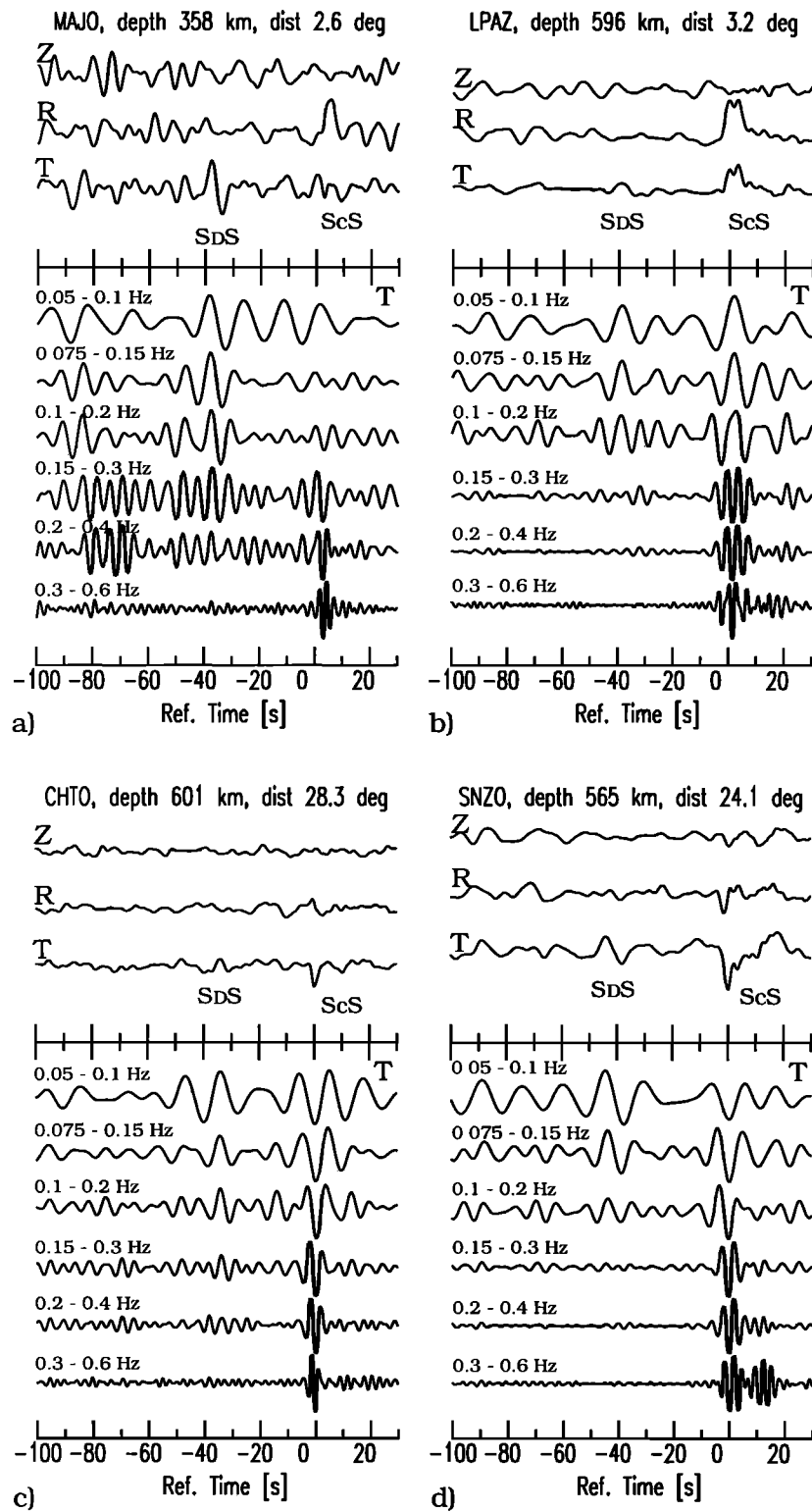
Figure 1. (upper panels) Three-component broadband seismograms at stations MAJO, LPAZ, CHTO, and SNZO aligned with respect to the theoretical ScS travel time. (lower panels) Transverse components band-passed at different frequencies and normalized per frequency band. A precursory signal SDS is visible at −35 to −55 s on each unfiltered transverse component. Notice the different epicentral distances and hypocentral depths (listed at the top of each figure).
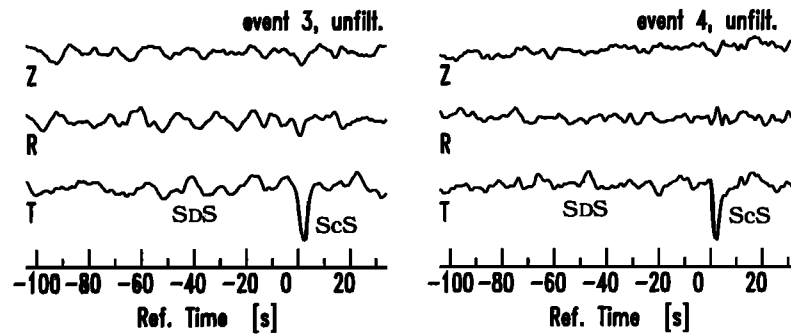
Figure 2. Three-component broadband seismograms at station SNZO for events 3 and 4 (see Table 1). S_DS and ScS are clearly visible on the transverse component.

Table 1. Events Used for the Detailed Study for Station SNZO

Event	Year	Day of Year	Longitude,°N	Latitude,°E	Depth,km	Dist,°
1	1993	314	-15.34	-177.03	381	26.9
2	1994	186	-16.30	-177.47	414	25.8
3	1993	114	-17.87	179.85	599	23.8
4	1994	19	-17.58	-178.50	533	24.4
5	1994	110	-17.80	-178.40	543	24.2
6	1993	106	-17.78	-178.86	565	24.1
7	1993	284	-17.85	-178.73	555	24.1
8	1993	080	-18.04	-178.53	589	23.9
9	1993	217	-18.10	-178.33	616	23.9
10	1994	68	-18.04	-178.41	563	23.9
11	1993	300	-18.28	-177.87	617	23.8
12	1993	92	-17.84	-177.07	362	24.4
13	1994	55	-17.42	-174.29	124	25.6
14	1994	56	-17.42	-174.27	121	25.6
15	1993	190	-19.78	-177.49	398	22.5
16	1993	91	-19.92	-177.54	406	22.3
17	1993	110	-20.88	-178.70	592	21.1
18	1994	114	-21.02	-178.69	584	21.0
19	1994	108	-21.41	-178.80	541	20.6
20	1993	233	-21.28	-178.02	427	20.9
21	1993	358	-21.85	-178.65	445	20.2
22	1994	90	-22.06	-179.53	580	19.8
23	1993	344	-22.18	-179.58	605	19.7
24	1992	217	-21.74	-177.21	253	20.7
25	1992	193	-22.48	-178.41	377	19.7
26	1992	317	-22.40	-178.10	360	19.8
27	1993	122	-21.15	-175.88	120	21.6
28	1993	90	-22.76	179.25	617	18.9
29	1993	56	-23.00	-177.22	166	18.5
30	1994	47	-26.27	178.27	606	15.3
31	1992	231	-28.64	-178.32	201	13.9
32	1994	139	-29.06	-178.38	258	13.5
33	1993	147	-29.36	-178.27	119	13.2
34	1994	116	-16.02	167.00	185	25.9
35	1994	124	-17.05	168.27	206	24.8
36	1994	42	-18.77	169.17	206	23.0
37	1992	285	-19.25	168.95	129	22.5

Underlined event numbers have similar $ScSH$ waveforms and were used for the stacks of Figures 7 and 8.

(and at steep ray incidence), this is not expected to exceed 0.03. Thus the amplitude of a steep-angle reflected S_DS phase should not be greater than the noise level. Indeed, in order to explain the large S_DS amplitudes and their polarity with respect to $ScSH$ with a reflection from a plane discontinuity in density alone entails a jump from about 5.5 to 9–10 g/cm^3; the latter values are generally recognized to describe the density of the top of the outer core. Therefore a focusing mechanism is required to explain the observed S_DS amplitudes, which greatly exceed 3% of the $ScSH$ phases. Even if the $ScSH$ phase was defocused, which would provide an overestimation of the S_DS amplitude with respect to $ScSH$, this would not explain the sometimes large S_DS signal-to-noise ratio.

Apart from the large amplitudes, we also observe frequency dependence. S_DS appears strongest in the band from 0.05 to 0.2 Hz (see Figure 1). Furthermore, the observed $S_DS/ScSH$ amplitude ratio decreases in the frequency band from 0.1 to 0.5 Hz. The recording from station MAJO (Figure 1a) is an exception. The absence of a low-frequent $ScSH$ could indicate structural complexity close to the CMB.
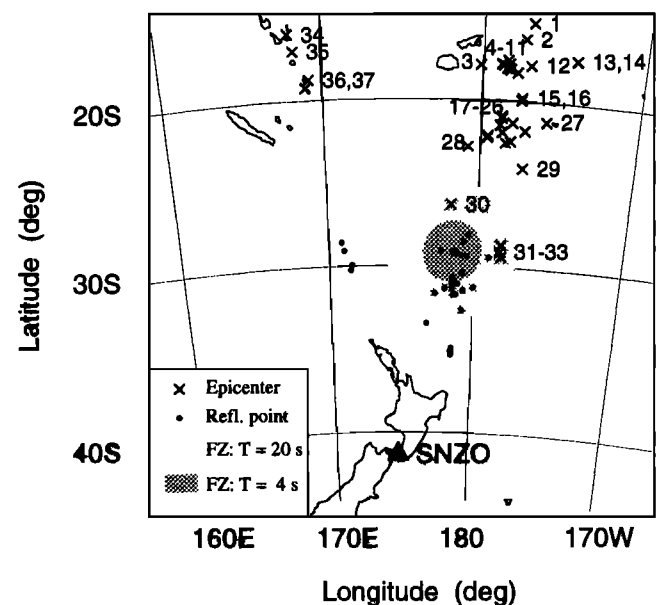

Figure 3. Event locations are marked by a cross and labeled with a number. The labels correspond to the event numbers of Table 1. Reflection points at the CMB are indicated by solids circles. The Fresnel zone at the CMB of event 6 for a period of 20 s is indicated by the light grey area. The corresponding 4-s period Fresnel zone is indicated by the dark grey area.
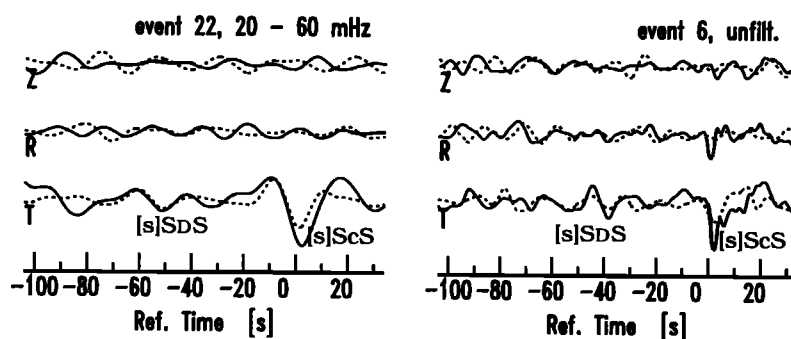
Figure 4. ScS (solid line) and sScS (dashed line) are aligned at 0 s and plotted on top of each other. The dashed transverse traces have been multiplied by −1.

Further, almost no precursory signal is observed at frequencies larger than 0.5 Hz. Alone, this frequency dependence can be modeled by a reflection from a linear transition zone 5–15 km wide vertically. However, given the large amplitudes, frequency-dependent focusing (which might also include a frequency-dependent reflection) is more likely.

In Figure 9, we show traces from two different events, aligned with respect to ScS and plotted on top of each other. The events are separated by 0.5°, and the separation of the geometrical reflection points is therefore approximately 0.3°. Whereas the solid trace (event 6) clearly shows a precursor at -45 s, there is less high-frequency signal evident on the other trace (event 10). As can be seen from Figure 1d, the precursor observed for event 6 is not visible at frequencies larger than 0.2 Hz. The Fresnel zone for a spherical reflector resembles a circle with a radius of ~1.9° for a frequency of 0.25 Hz (see Figure 3). Here the Fresnel zone is defined by $\Delta t \leq \frac{1}{4}T$, where T is the period and Δt is the travel time residual between rays with perturbed and geometrical bounce points. Thus events 6 and 10 show that SDS/ScSH amplitude ratios in the frequency band from 0.05 to 0.2 Hz may vary for different reflection points located within the same two-dimensional (2-D) Fresnel zone. These observations support the focusing model since they cannot be explained by radial one-dimensional (1-D) layering above the CMB. Frequency-dependent focusing and defocusing can occur for different reflection points within the same Fresnel zone. In other words, it looks like that station SNZO was closer to a region of focusing for event 6 than for event 10. This might explain the presence and absence of the high-frequent components of the focused wave field for the events 6 and 10.

In the presence of topography, signal from the SDS precursor is also expected on the radial component. Its amplitude will depend on the source radiation pattern as well as the actual shape of topography. Indeed, some signal is visible on the radial component of the stacked records of Figure 8. This signal is more difficult to identify on the individual seismograms, but a hint of it might be recognized, e.g., for event 6 in Figure 1d. In the following we are mainly going to discuss the occasionally strong energy on the transverse component. However, any proposed model must also explain the SDS energy on the radial component.

Synthetic Modeling

As established above, a focusing mechanism is necessary to explain large SDS amplitudes and the variability of the observations with a reasonable velocity and density contrast. There are many ways to focus a wave field through a three-dimensional (3-D) Earth structure, and the subject of the following section is to investigate one possibility which we find to be effective: focusing through a discontinuity with topography. This approach is further justified by observations of near-grazing ScS precursors that show a variable depth to this discontinuity [e.g., Garnero et al., 1993; Kendall and Shearer, 1994].

The Method

We chose a Kirchhoff-Helmholtz -related method after Frazer and Sen [1985] and Frazer [1987] which has been successfully applied for $P_{410}P$ by Neele and Snieder [1992] and $P_{660}s$ phases
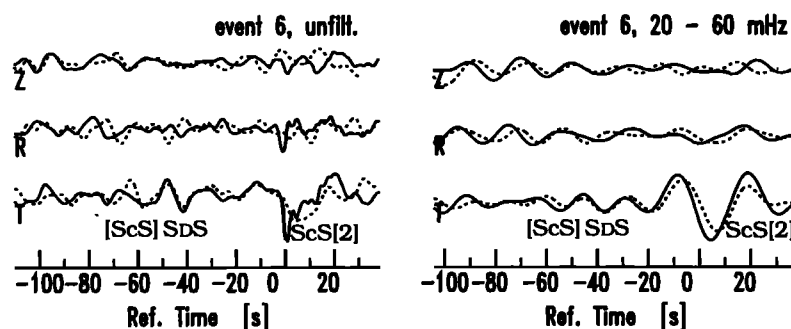

Figure 5. ScS (solid line) and ScS2 (dashed line) are aligned to 0 s and plotted on top of each other. The dashed traces with ScS2 have been multiplied by 3. The seismograms on the left are unfiltered and on the right are band-passed between 20 and 60 mHz.
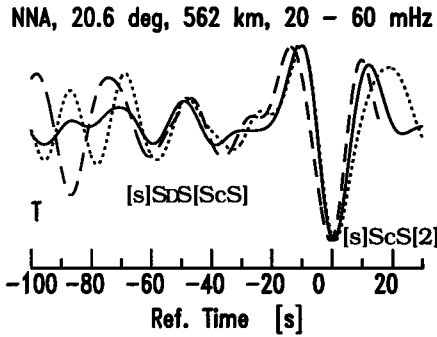
Figure 6. *ScS* (solid line), *sScS* (dotted line) and *ScS2* (dashed line) are aligned to 0 s, band-passed between 20 and 60 mHz, and normalized. The trace with *sScS* has been multiplied by -1. Station is NNA (Peru), epicentral distance and hypocentral depth are $20.6°$ and 562 km, respectively. Precursors to all three phases are coherent at low frequencies.

by *Van der Lee et al.* [1994]. It is essentially a combination of geometrical acoustics and plane wave reflections with the Kirchhoff-Helmholtz formulation as its backbone. Geometrical optics are used to propagate the rays between the source, discontinuity and station, and the plane wave *SH*- and *SV*-reflection coefficients are incorporated to construct a generalized reflection coefficient. We are using the single fold representation [*Frazer and Sen*, 1985], which means that we integrate over just one surface. This is either the CMB or the reflector above the CMB. The final seismograms are obtained by summing both time series. Thus the *ScS* phase is calculated for the unperturbed medium. The geometry and the laterally homogeneous background medium ensure that the wave field does not have a caustic on the reflector, which implies that there is no singularity in the integration. However, caustics at the receiver are allowed since the Kirchhoff-Helmholtz theory treats the receiver as a second source of a second wave field. Owing to the use of plane wave reflection coefficients, the method is restricted to plane waves and a local plane interface. Consequently, the scale length of the topography has to be larger than the actual Fresnel zone.
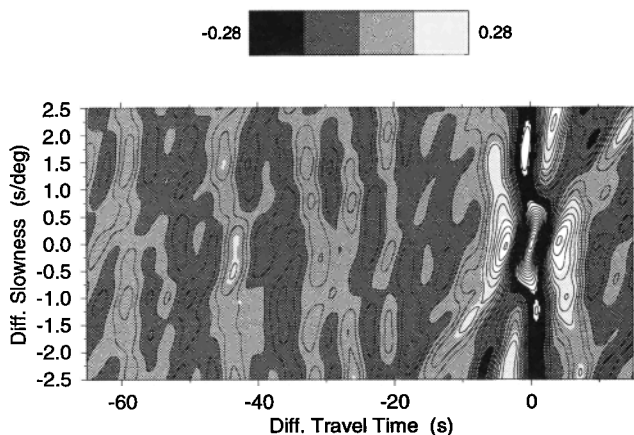

Figure 7. Normalized slant stack for 18 transverse seismograms. Shaded contouring ranges from -0.28 to 0.28, while the lines contour all amplitudes with a step size of 0.05. *ScSH* is visible as minimum at $\Delta t = 0$ s, $\Delta p = 0$ s/deg. The precursor with positive amplitude is evident at $\Delta t = -43$ s and $\Delta p \simeq -0.5$ s/deg.
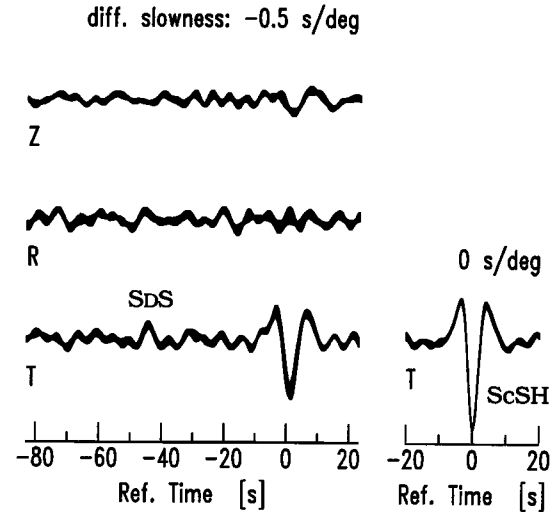

Figure 8. Slant-stacked seismograms for a differential slowness of -0.5 s/deg. The precursor at -43 s is mainly transversely polarized and has opposite polarity to *ScSH*. The one standard deviation uncertainty is indicated by the line thickness. The stacked wavelet to the right shows the *ScSH* signal at zero slowness.

For the synthetics, we used a station-event configuration as illustrated in Figure 10. The epicentral distance from event 0 (in the southeastern corner) and the receiver is $25°$. The event cluster consists of 16 more events, 8 to the west (W1–W8) and 8 to the north (N1–N8). The spacings between the hypocenters are $0.5°$ (W1–W4, N1–N4) and $0.1°$ (W5–W8, N5–N8). We used an egg-box-shaped topography schematically indicated by the shading in Figure 10. One of the minima of the topography is fixed at the position of the geometrical bounce point for event 0, while topography amplitude A and scale length λ are free parameters which vary the topography. A is measured from a mean depth to its extremum. Whether the wave field for a fixed station-event configuration is focused or not depends on the frequency, i.e., Fresnel zone resolution width, and the curvature of the topography, which is determined by A and λ. In other words, there exists a trade-off between A and λ for fixed frequencies, which consequently complicates distinguishing between certain models.

For our test calculations, we used a discontinuity with an S-velocity and density increase of 3%. This means that the SH-wave reflection coefficient and impedance increase are -0.03 and 6% at normal incidence. The synthetic seismograms are calculated for frequencies up to 1 Hz. The source has a spherically symmetric radiation pattern with a delta-function source. We expect focusing for scale lengths λ larger than the Fresnel zone, but not too large, because then the curvature of the topography gets too small for focusing. If the scale length is much smaller than the Fresnel zone resolution width, the effect of topography is expected to average out, but this cannot be tested by our method due to the plane wave restriction.

The Results

1. The most important result is that it is possible to focus the wave field of the *SᴅS* phase to obtain the observed large amplitude *SᴅS* phases by assuming a fairly moderate discontinuity. In the three leftmost panels of Figure 11, we show the results for a 3%
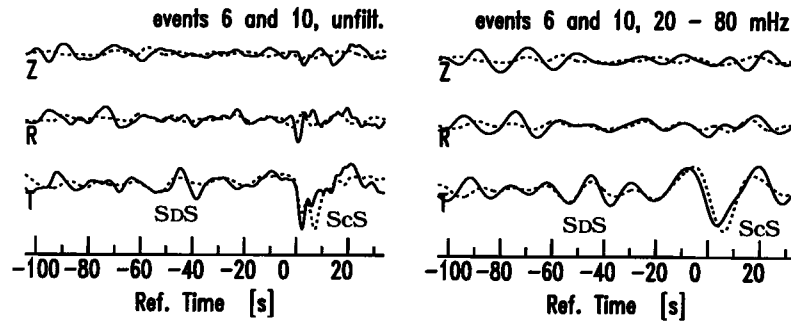
Figure 9. Two seismograms aligned with respect to the *ScSH* phase and plotted on top of each other. The seismograms to the left are unfiltered and to the right are band-passed. Event locations are separated by about $0.5°$.

discontinuity in S-velocity and density, with amplitude $A = 35$ km, and varying scale lengths and frequency ranges. The event 0 - station configuration (Figure 10) has been used for these calculations. The amplitudes at high frequency indicate strongest focusing at about $\lambda = 20°$–$21°$ ($\simeq$1200 km). Other tests showed that decreasing the event 0 – station distance from $25°$ to $20°$ leads to amplitudes further increased by about 35%. The most important reasons for this are that (1) the SH-reflection coefficient varies as a function of incidence angle and (2) focusing depends on the configuration of event, station, and topography.

2. There exists a strong trade-off between topography amplitude (A) and scale length (λ). If A is increased, focusing is obtained

for larger scale lengths, and if A is decreased, smaller scale lengths lead to focusing. Similar focused S_DS amplitudes for the frequency range smaller than 1 Hz are attained for scale lengths and amplitudes between $\lambda = 19°$, $A = 30$ km and $\lambda = 25°$, $A = 50$ km. Outside this range of topography, the focused amplitudes decrease. Two examples of lower-amplitude focusing can be found in the fourth panel of Figure 11. The trade-off between A and λ can be approximated by considering the theoretical focusing factor [*Neele and Snieder*, 1992], which is the spectral ratio of the wave fields from a perturbed and a flat reflector. Assuming that the focused amplitudes belong to one single stationary phase, the focusing factor becomes a function of A/λ^2. This is what we approximately find from our synthetics for models which cause strong amplitude focusing.

3. In Figure 12, we show the seismograms for the event cluster of Figure 10 and demonstrate the spatial sensitivity of the focused wave field. The parameters of the topography used are $A = 35$ km and $\lambda = 20°$. High-frequency reflections are only observed within a small focusing region, while low-frequency reflections occur over a wider region. It appears that within the frequency range we consider, the caustic volume decreases with increasing frequency. Here the caustic volume refers to the finite caustic for physical rays at finite frequencies [*Kravtsov*, 1988]. It is not expected that the caustic volume generally decreases with increasing frequencies. For instance, rays with Fresnel zones much smaller than the scale length of our topography locally sample an almost plane-like reflector which does not lead to focusing. Alternatively, waves with decreasing frequencies cannot always have an increased caustic volume, since for scale lengths much smaller than the Fresnel zone, the effect of the topography on the wave field averages out to zero.

4. Figure 12 further shows that a variation of event position less than $2°$ (see W1 and N1) is enough to move out of the S_DS focusing region for all frequencies. The corresponding reflection point separation is surely smaller than $1°$, and Figure 12 therefore illustrates amplitude variations which might occur for geometrical bounce points clustered within the same 2-D Fresnel zone. A Fresnel zone with radius larger than $2°$ corresponds to waves with frequencies smaller than 0.25 Hz. This implies that small-scale structures are not required to explain amplitude variations within a Fresnel zone. This is mainly due to two reasons: (1) The distance from the reflector to the Earth's surface is large, which allows the wave field to have caustics close to the receiver caused by large-scale structures at the reflector and (2) the width of these caustic volumes is small.
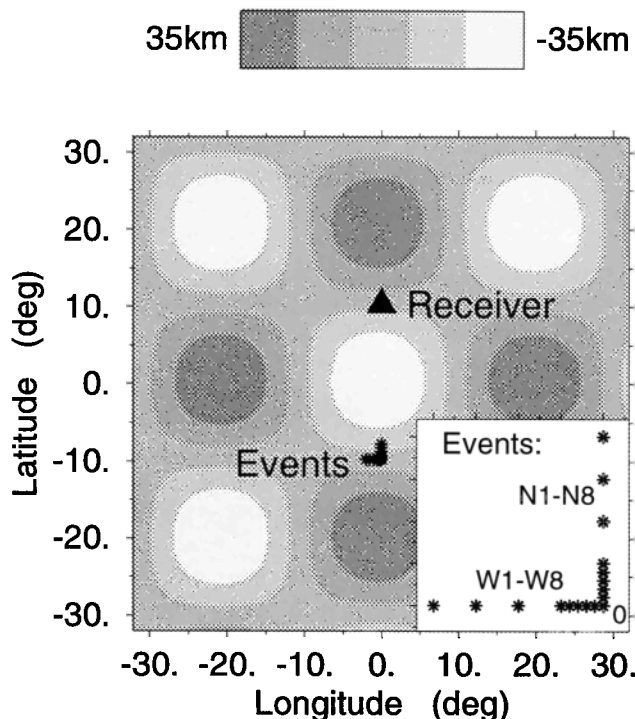

Figure 10. Station-event configuration projected on top of the schematically indicated egg-box like topography with scale length $20°$ at D''. The enlarged event cluster is shown in the insert at the lower right. The event at the corner is labeled event 0, and its distance to the receiver is $25°$. Some events have a spacing of $0.5°$, others of $0.1°$. Events W1 and N1 are separated by $2°$ from event 0.
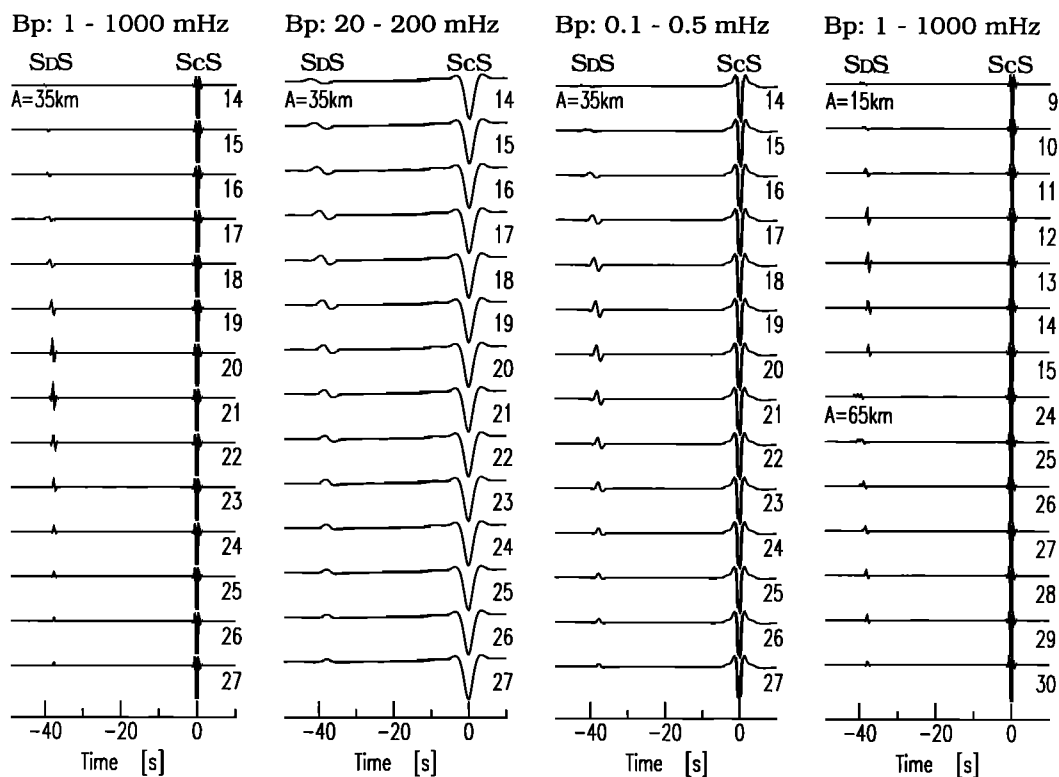
Figure 11. Transverse synthetic seismograms which have been calculated for the event 0 - station configuration (Figure 10). The number to the lower right of each trace shows the scale length λ (in degrees) used. The amplitude A was fixed to 35 km (the first three columns), 15 km (the fourth column, top 7 traces), and 65 km (the fourth column, lower 7 traces).

5. The calculated waveforms for SDS have similarities to our data. The synthetic SDS waveforms have opposite polarity to the ScS phase when no strong focusing occurs. Thus they are dominated by the impedance increase (compare with Figure 8). In the strong focusing region itself, the SDS waveforms are more complex. They do not resemble the ScS waveform but look more like its negative Hilbert transform. This involves a negative reflection coefficient and the phase retardation of $\pi/2$ at a caustic. Note that these ScS and SDS waveforms from trace 6 in Figure 9 approximately resemble the synthetic waveforms.

We show that focusing due to large-scale topography (1200–1600 km) of a moderate discontinuity can explain the intermittently observed large SDS amplitudes. The frequency-dependent focusing depends on amplitude A and wavelength λ of the topography, vertical distance between discontinuity and receiver, the event-receiver configuration itself, and the event-receiver position relative to the topography. The small spatial sampling of the wave field and the trade-off, ambiguity, and complexity of the focusing mechanism make it difficult to further constrain the model. Indeed, we find that a SDS amplitude decrease with increasing frequency (the observed frequency cut off at 0.5 Hz) can be explained by any combination of the three following circumstances: (1) The reflection coefficient is frequency dependent if the reflector is not a single first-order discontinuity. (A first-order discontinuity is a transition where the elastic parameters and/or density change discontinuously.) (2) The Fresnel zone which decreases with increasing frequency leads to a smaller sampling of the curved reflector for higher frequencies and will at one point lead to a decrease of focusing. (3) The caustic

volume or focusing region gets smaller with increasing frequency. Thus any phase in the vicinity of a caustic volume will show a frequency dependence with a "fading out" of higher frequencies.

In our calculations, we considered a monochromatic sinusoidal reflector only. Structure with more scale lengths will further increase the ambiguity. For instance, assume that there is a small-scale bump superimposed on the minimum of the sinusoidally shaped reflector. If in addition the location of this bump coincides with the geometrical reflection point, then a high-frequency wave will be defocused while the low-frequency components are still focused due to the long-scale structure. We expect to observe a low-frequent precursor. Alternatively, high-frequent SDS focusing could also have been suppressed by a frequency-dependent reflection coefficient and/or by having the receiver in the vicinity of the focusing zone as mentioned above.

Note that we can increase the synthetic $SDS/ScSH$ amplitude ratio even more by replacing the monochromatic sinusoidally shaped topography with a parabolic reflector which strengthens SDS or by defocusing the $ScSH$ phase by CMB topography. We cannot resolve all the ambiguities with the present amount of data, and we refrain from presenting a "best" model.

Last, we want to point out that our synthetic SDS phases have amplitudes on the radial component which are 60–70% of those on the transverse component. This is expected due to the smaller SV-reflection coefficient (it may even change sign) when compared with the SH-reflection coefficient for the considered slowness range. Note that the observed radial-to-transverse SDS amplitude ratio of Figure 8 is similar to the synthetically calculated one.
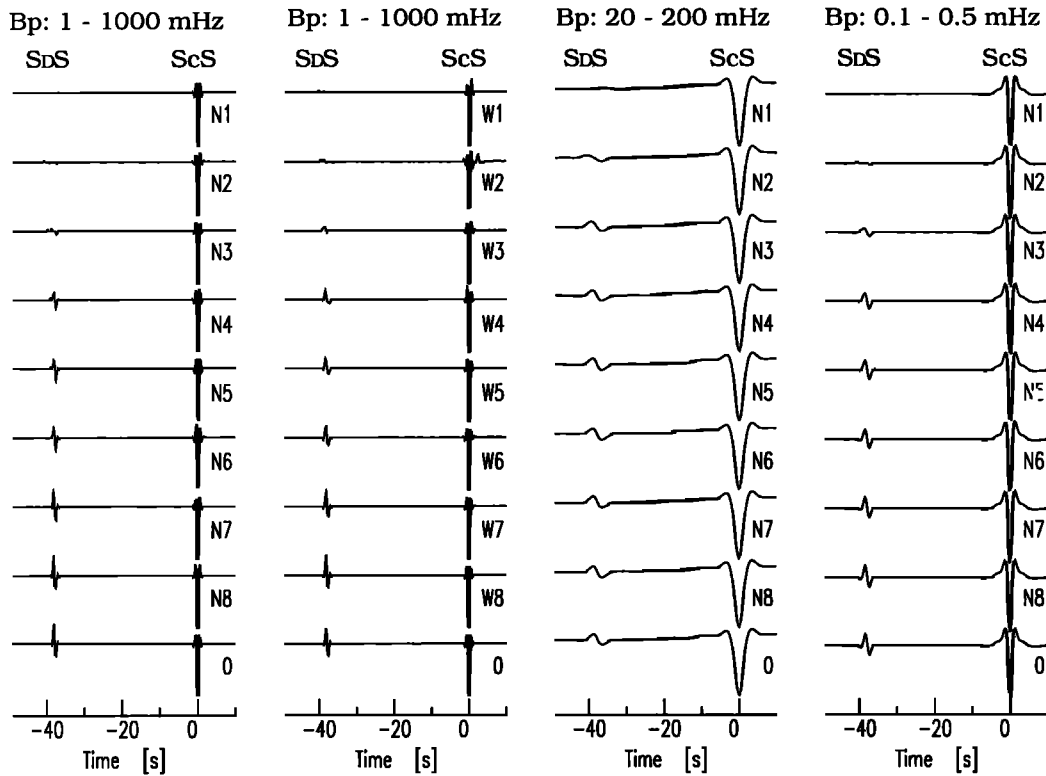
Figure 12. Synthetic seismograms which have been calculated for the event configuration of Figure 10. Topography used has an amplitude $A=35$ km and scale length $\lambda=20°$. The event spacing between N1–N2, N2–N3, and N3–N4 (W1–W2, ..., analogous) is $0.5°$, and all the other event locations are separated by $0.1°$. The epicentral distance of event 0 to the receiver is $25°$. The frequency band of the traces is indicated at the top of each panel.

Discussion

We observe intermittent ScS and sScS precursors at different stations, which we interpret to be caused by a reflector located at about 180 km above the CMB. We can rule out other possible interpretations for S$_D$S such as near-source or near-receiver scattering. Our more detailed analysis shows the precursors for a reflector underneath the Kermadec region. The depth of the reflector is constrained by the differential travel time $(t_{ScS} - t_{S_DS})$ to about 180 km. This depth estimation is based on the assumption that the lowermost 180 km can be described by a constant S-velocity of 7.26 km/s. A velocity perturbation of $\pm5\%$ would lead to a change in depth estimation of about ±10 km.

The large S$_D$S/ScSH amplitude ratio and the frequency dependence of the observations require frequency-dependent focusing of S$_D$S. We tested focusing using topography, and synthetic modeling shows that realistic models can focus the wave field strongly enough to be observed. The S$_D$S/ScSH amplitude ratio from the synthetics from a monochrome sinusoidal topography reach 1/3, which is the ratio of the stacked phases from Figure 8. Still, we need to increase this amplitude ratio in order to explain the upper bound of S$_D$S/ScSH observed in individual traces such as presented in Figures 1 and 2. This can be done in two ways: first, by defocusing the ScS phase due to D" heterogeneities and/or CMB topography and second, by further focusing S$_D$S. We cannot resolve this ambiguity by the presented amount of data but expect topography with dominant scale lengths on the order of $19°-25°$ (that is, 1200–1600 km at the reflector) with corresponding amplitudes of 30–50 km. We showed

that such topography could lead to intermittent observations of S$_D$S.

The inferred long-scale structures further agree with the mapped ScS-S and sScS-sS differential travel times by *Wysession et al.* [1994] or the multiple-phase analysis by *Young and Lay* [1990]. *Wysession et al.* [1994] find anomalies with dominant lateral dimensions of about 1000–2500 km or more beneath the west Pacific for the lowermost 300 km of the mantle in a study which could resolve much smaller scale lengths.

Furthermore, the depth of the reflector presented here, 180 km, is in good agreement with a ScS precursor found by *Gaherty and Lay* [1992] and *Garnero et al.* [1993] for near-grazing S waves under Eurasia and the mid-Pacific D" region, respectively. Also, SV diffracted waves around the Earth's core underneath Alaska can be best modeled by a discontinuity at a depth 180 km above the CMB [*Lay and Young*, 1991]. Our estimated topography of 30–50 km would result in a scatter in differential travel times of 2–5 s, which is consistent with observations by *Gaherty and Lay* [1992]. The intermittent observation of their 160-km precursor caused *Gaherty and Lay* [1992] to assume that its spatial extension is limited. We suspect, however, that the intermittent character of their wide-angle observations has a cause similar to the steeply reflected precursors of our study, i.e., focusing and defocusing due to topography.

A similar mechanism could also explain the clustering within a Fresnel zone of observable and unobservable precursors from the top of the D" (at approximately 300 km above the CMB). Such observations have been reported by *Weber* [1993] for broadband S$_D$S and P$_D$P. *Weber* [1993] finds reflector spots as small as 130 km, while reflectors as large as 1500 km have also been inferred [e.g.,

Young and Lay, 1990]. This does not contradict our suggestion of focusing, since *Young and Lay* [1990] used long-period data, while *Weber* [1993] worked with broadband data with dominant periods of 4–6 s for *SDS* and 1 s for *PDP* waves. We demonstrated that topography of large scale lengths causes highly variable short-period reflections observed in small focusing regions and more stable long-period reflections in larger focusing regions. Consequently, the top of the D" at ~300 km, as both studies bring out, can be explained by a global reflector, which is dominated by relatively large scale lengths. Indeed, *Nataf and Houard* [1993] proposed a global discontinuity on top of D" which, due to laterally varying properties, leads to intermittent detection.

Evidence for a *P* wave discontinuity at 160 km above the CMB, a depth similar to our *S* wave reflector, has furthermore been presented by *Wright et al.* [1985] from short-period data using different arrays and source regions. They used travel time and slowness measurements of low-angle reflected *PDP* phase underneath Indonesia, western Pacific, and mid-Pacific. On the other hand, *Neuberg and Wahr* [1991], searching for high-frequency *PDP* phases steeply reflected from one small spot between Tonga and Australia, did not see such a discontinuity. However, *H.-C. Nataf* (personal communication, 1996) observed steeply reflected *PDP* phases from the top of D" underneath Alaska.

Steep incidence *ScS* reverberations were considered by *Revenaugh and Jordan* [1989]. They observed a reflector which, due to ambiguity inherent to their method, could be caused either by a rapid impedance decrease in the upper 100 km of the mantle or by an impedance increase (R ~ −0.03) about 170 km above the CMB. The latter possibility is consistent in polarity and depth with our observations. *Revenaugh and Jordan* [1989] used 40 mHz low-passed data, which are much less affected by focusing than the higher frequencies used here. This explains their impedance increase of about 6%, which is much less than we would find from the focused phases by assuming plane layering and higher frequencies. In a more extensive study, *Revenaugh and Jordan* [1991] gave no evidence for the discontinuity 170 km above CMB.

Conclusions

We have found intermittent observations of *ScSH* precursors recorded at small epicentral distances ($\Delta < 30°$) and conclude that these are steeply reflected phases from a reflector located at about 180 km above the CMB. With evidence from synthetic seismograms for steeply reflected *S* waves, we infer that topography with scale lengths of about 1200–1600 km can explain the observed frequency-amplitude characteristics of the precursor. We do not exclude the presence of shorter scale length structure but find that (at least for steep incidence reflections) the observation of intermittent phases and the interpretation of reflector spots smaller than the Fresnel zone can be explained by long-scale topography. Owing to a limited data set, we can give no evidence for a global presence of the reflector described here. However, we believe that the D" is at least locally layered.

The frequency dependence of focusing can be understood as a combination of three processes. These are (1) the frequency-dependent size of the caustic volume, (2) the different sampling of the curved discontinuity due to the frequency-dependent Fresnel zone, and (3) a frequency-dependent reflection coefficient. The ambiguity in the interpretation and separation of these effects can

probably be decreased with good spatial sampling of the focused wave field. Altogether, more broadband data and 3-D modeling for a broad frequency range are required for a better understanding of the radial structure of D".

References

Bullen, K.E., An Earth model based on a compressibility pressure hypothesis and the Earth's interior, *Mon. Not. R. Astron. Soc. Geophys. Suppl., 6*, 50-59, 1950.

Cormier, V.F., Some problems with *S, SKS* and *ScS* observations and implications for the structure of the base of the mantle and the outer core, *J. Geophys., 57*, 14-22, 1985.

Doornbos, D.J., and J.C. Mondt, *P* and *S* waves diffracted around the core and the velocity structure at the base of the mantle, *Geophys. J. R. Astron. Soc., 57*, 381-395, 1979.

Frazer, L.N., Synthetic seismograms using multifold path integrals - 1. Theory, *Geophys. J. R. Astron. Soc., 88*, 621-646, 1987.

Frazer, L.N., and M.K. Sen, Kirchhoff-Helmholtz reflection seismograms in a laterally inhomogeneous multi-layered elastic medium - 1. Theory, *Geophys. J. R. Astron. Soc., 80*, 121-147, 1985.

Gaherty, J.B., and T. Lay, Investigation of laterally heterogeneous shear velocity structure in D" beneath Eurasia, *J. Geophys. Res., 97*, 417-436, 1992.

Garnero, E., D. Helmberger, and S.P. Grand, Preliminary evidence for a lower mantle shear wave velocity discontinuity beneath the central Pacific, *Phys. Earth Planet. Inter., 79*, 335-347, 1993.

Haddon, R.A W., and G.G.R. Buchbinder, *S* wave scattering by 3-D heterogeneities at the base of the mantle, *Geophys. Res. Lett., 14*, 891-894, 1987.

Kendall, J.M., and P.M. Shearer, Lateral variations in D" thickness from long-period shear wave data, *J. Geophys. Res , 99*, 11,575-11,590, 1994.

Kravtsov, Y.A., Rays and caustics as physical objects, in Progress in Optics 26, edited by E. Wolf, pp.229-348, Elsevier Science, New York, 1988.

Lay, T., Structure of the core-mantle transition zone: A chemical and thermal boundary layer, *Eos Trans. AGU, 70*, 49, 1989.

Lay, T., and D. Helmberger, A lower mantle *S* wave triplication and the shear velocity structure of D", *Geophys. J. R. Astron. Soc., 75*, 799-837, 1983.

Lay, T., and C J. Young, Analysis of seismic *SV* waves in the core's penumbra, *Geophys. Res Lett., 18*, 1373-1376, 1991.

Loper, D.E., and T. Lay, The core-mantle boundary region, *J Geophys. Res., 100*, 6397-6420, 1995.

Mitchell, B., and D. Helmberger, Shear velocities at the base of the mantle from observations of *S* and *ScS, J. Geophys. Res., 78*, 6009-6020, 1973.

Nataf, H-C., and S. Houard, Seismic discontinuities at the top of D": A world-wide feature?, *Geophys. Res. Lett., 20*, 2371-2374, 1993.

Neele, F., and R. Snieder, Topography of the 400 km discontinuity from observations of long period *P400P* phases, *Geophys. J Int., 109*, 670-682, 1992.

Neuberg, J., and J. Wahr, Detailed investigation of a spot on the core-mantle boundary using digital PcP data, Phys. Earth Planet. Inter., 68, 132-143, 1991.

Revenaugh, J., and T H. Jordan, A study of mantle layering beneath the western Pacific, J. Geophys. Res., 94, 5787-5813, 1989.

Revenaugh, J., and T.H Jordan, Mantle layering from ScS Reverberations, 4, The lower mantle and core-mantle boundary, J. Geophys. Res., 96, 19,811-19,824, 1991

Schlittenhardt, J., J. Schweitzer, and G. Müller, Evidence against a discontinuity at the top of the D", Geophys. J. R. Astron. Soc, 81, 295-306, 1985.

Van der Lee, S , H. Paulssen, and G. Nolet, Variability of P660s phases as a consequence of topography of the 660 km discontinuity, Phys. Earth Planet. Inter., 86, 147-164, 1994.

Weber, M., P and S wave reflections from anomalies in the lowermost mantle, Geophys. J. Int., 115, 183-210, 1993.

Weber, M., and J.P. Davis, Evidence for a laterally variable lower structure from P- and S-waves, Geophys. J. Int., 102, 231-255, 1990.

Wright, C., K.J. Muirhead, and A.E. Dixon, The P wave velocity structure near the base of the mantle, J. Geophys. Res., 90, 623-634, 1985.

Wysession, M.E., L. Bartko, and J. Wilson, Mapping the lowermost mantle using core-reflected shear waves, J. Geophys. Res, 99, 13,667-13,684, 1994.

Young, C J., and T. Lay, The core-mantle boundary, Annu. Rev. Earth Planet Sci, 15, 25-46, 1987.

Young, C.J., and T. Lay, Multiple phase analysis of the shear velocity structure in the D" region beneath Alaska, J. Geophys. Res., 95, 17,385-17,402, 1990.

H. Paulssen and M. Schimmel, Department of Theoretical Geophysics, Institute of Earth Sciences, Utrecht University, P.O. Box 80.021, Budapestlaan 4, 3508 TA Utrecht, Netherlands. (email: schimmel@geof.ruu.nl; paulssen@geof.ruu.nl)